Optimisation of copper electroforming for manufacturing superconducting radiofrequency cavity substrates

L. Lain Amador[1*], L. M. A. Ferreira[1], M. Taborelli[1]
1. CERN, Geneva, Switzerland
*lucia.lain.amador@cern.ch

Abstract

In the framework of the Future Circular Collider (FCC) study, SRF (Superconducting Radio Frequency) cavities will be produced by applying niobium superconducting thin films onto copper substrate cavities. A seamless process, which guarantees a high quality Cu substrate and a very smooth surface finishing, would be an advantage. In the present innovative approach, seamless model cavities are produced by copper electroforming on a sacrificial aluminium mandrel. Since the cavity works under vacuum, it must withstand the force of the atmospheric pressure and the thickness of the copper layer should guarantee everywhere the mechanical robustness. COMSOL® simulations, exploiting the electrochemistry module, were performed in order to optimise the copper thickness uniformity along the cavity. A combination of secondary anodes and masking was proposed to achieve a minimum thickness of 2 mm everywhere and to decrease the plating time. The simulations were run with a moving mesh in order to simulate the boundary displacement resulting from the plating on the cathode and the consumption of the secondary anodes. Finally, the resulting optimised geometry of anode and masking highly improves the copper layer thickness uniformity along the cavity.

1. Introduction

The Future Circular Collider study (FCC) is developing designs for the next generation particle collider after LHC. Within the project, the superconducting radiofrequency cavities will be produced by applying niobium superconducting thin films onto copper substrate cavities.

Nb coated SRF cavities are presently used at CERN in the Large Hadron Collider (LHC) and in the Quarter Wave Resonators (QWRs) of ISOLDE beam facility [1]. The copper elliptical cavity substrates are normally produced by mechanical forming several subcomponents as half cells and cut-offs, which are assembled together by electron-beam welding. Figure 1 presents the nomenclature of a basic elliptical cavity. The presence of the weld groove in the most critical place of the cavity (equator) has been identified as a imitation for the RF performance [2]. Therefore, a seamless process, able to produce the entire cell of the cavity without the use of welding, is highly desirable.

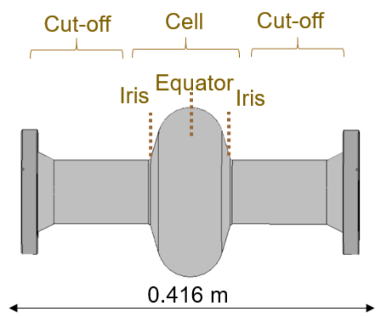

Figure 1. 1.3 GHz SRF cavity nomenclature.

Seamless cavities have been approached by different methods over the last decade [3]. In this work, the copper cavity is produced by copper electroforming on an aluminium mandrel, which has the shape of the cavity inner surface. Firstly, a thin copper film is coated on the degreased mandrel in order to provide adherence for the electroplating step [4]. The copper coating is performed by direct current magnetron sputtering on the aluminium mandrel using Kr ($8x10^{-4}$ mbar) as process gas. Afterwards, the stainless steel flanges are assembled mechanically to the coated mandrel and the whole body is prepared for electroplating [4]. A copper acidic sulphate bath is used to plate 2 mm of copper layer thickness at an average current density of 1.6 A/dm^2. The plating is performed in pulses of 7 ms on-time and 8 ms off-time. The bath contains six copper flat anodes that are located lengthwise on both sides of the bath. The geometry of the electroplating bath and the cavity is shown in Figure 2.

The bottleneck of the process is the uneven thickness distribution of the plated layer along the complex shape of the cavity. The aim of this work is to simulate and optimise the electroforming process by using COMSOL Multiphysics®. In this paper, a way to improve thickness uniformity is presented, which uses secondary anodes positioned at the iris to promote plating and a mask at the equator to reduce the deposition.

COMSOL simulations were used to assess voltage, local current density and plated thickness along the cavity. Parameter sweep was used in order to find the optimum distance and geometry of the secondary anodes. The boundary displacements resulting from the plated thickness at the cathode and the anodic dissolution were simulated thanks to a moving mesh. In addition, the primary and secondary anodes were independently controlled using two power supplies.

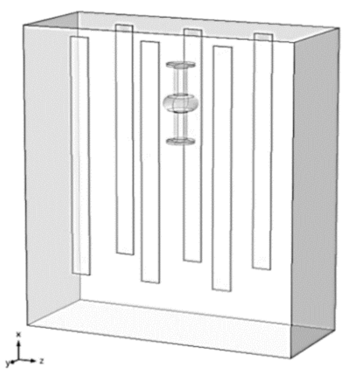

Figure 2. Geometry of the cavity and the electroplating bath as seen in COMSOL.

2. Simulations Methodology

The current density distribution in the cavity was modelled with COMSOL Multiphysics® using the Secondary Current Distribution (SCD) physics module.

The electron transfer reactions that take place at the anode and cathode are the following assuming a 100% yield:

Anode: $Cu \rightarrow Cu^{2+} + 2e^-$

Cathode: $Cu^{2+} + 2e^- \rightarrow Cu$

The electrolyte is well stirred during the whole process. Therefore, in absence of concentration gradients, the relationship between the local current density (i_m) and the local potential derivative ($\boldsymbol{\nabla \emptyset_m}$) is described by the Ohm's law.

$$i_s = -\sigma_s \nabla \emptyset_s \qquad \text{[Electrode, s]}$$

$$i_l = -\sigma_l \nabla \emptyset_l \qquad \text{[Electrolyte, l]}$$

Where σs is the conductivity at the electrode and σ_l is the conductivity of the electrolyte. The activation overpotential (η_{Cu}) is the difference between the actual potential difference and the equilibrium potential ($E_{eq,Cu}$).

$$\eta_{Cu} = \emptyset_s - \emptyset_l - E_{eq,Cu}$$

The secondary current takes into account the effect of electrode kinetics and the bath resistance. It neglects the influence of concentration variations in the electrode kinetics. The local current at the electrode surface follows the Butler-Volmer equation.

$$i_{loc,Cu} = i_{0,Cu}\left(exp\left(\frac{\alpha_a \cdot F \cdot \eta_{Cu}}{R \cdot T}\right) - exp\left(\frac{-\alpha_c \cdot F \cdot \eta_{Cu}}{R \cdot T}\right)\right)$$

Where $i_{loc,Cu}$ is the local current density, $i_{0,Cu}$ is the exchange current density, T is the temperature, R is the universal gas constant, F is the Faraday constant and α_c and α_a are the transfer coefficients for the cathodic and anodic reaction, respectively. In the case of a symmetric reaction, the sum of both is equal to unity. The kinetic parameters and electrolyte properties are given in Table 1.

Table 1 Kinetics parameters and electrolyte properties

$i_{0,Cu}$ (A/m^2)	0.1
α_c	0.5
$E_{eq,Cu}$ (v)	0.33
$CuSO_4$ (M)	0.5
Conductivity σ (S/m)	15
Temperature (K)	298

The rate of deposition at the cathode boundary surface and the rate of dissolution at the anode boundary are calculated according to:

$$v = \frac{i_{loc,Cu}}{n \cdot F} \cdot \frac{M}{\rho}$$

Where M is the molar mass of the deposited metal (63.35 g/mol), ρ is the density (8.96 g/cm^3) and n the number of electrons exchanged in the reaction (2 electrons).

3. Simulation Results

The simulations were run using a 3D model of the plating bath and the cavity mandrel and using the same electroplating parameters that were used experimentally to produce the test cavities. The plated thickness on the experimental cavities was measured by means of an Olympus Magma-like 8600 thickness gauge. The measured thickness and the ones obtained by simulation are presented in Figure 3. The plating time for the test cavities varied from 76 hours (orange, D2) to 180 hours (red, D3) and the simulation was extended to 300 hours (blue).

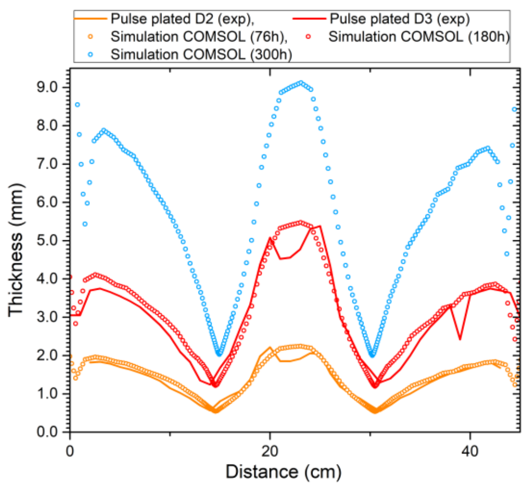

Figure 3. Thickness distribution along the cavity. Experimental results and simulation.

The simulated thickness obtained from COMSOL agrees with the experimental plating thickness. The maximum thickness is found at the equator of the cavity and the minimum at the iris. The ratio between the maximum and the minimum thickness is 3.5 and 4.1, for the orange and red curves, respectively. Although the deviation from the experimental results is larger for longer times, it is sufficiently robust to validate our simulation model. With the present setup it would be necessary to run the electroplating process for 300 hours to achieve a minimum thickness of 2 mm across the whole geometry achieving an even worse thickness ratio of 4.6.

To tackle the huge unevenness ratio, it was necessary to improve the plating rate near the iris, while refraining at the equator. Thus, a scheme with mask and secondary anodes was designed and is shown in Figure 4. The central mask is a ring of 40 mm height, 2 mm thickness and 165 mm internal diameter that covers the equator. The secondary anodes are copper rings with a cross section of 35 mm by 20 mm and 145 mm internal diameter. The location of the secondary anodes with respect of the mask (Xa in the design) is very important, as it defines the distance from the copper anode to the iris and equator. In addition, two non-conductive disks are used below the secondary anodes to mask the anode surface that is directly exposed to the equator of the cavity, preventing higher plating rates at the equator.

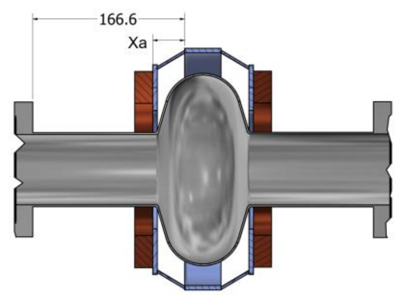

Figure 4 Proposed mask design (cross-sectional cut). The position of the copper anodes ring with respect of the support is optimised, Xa.

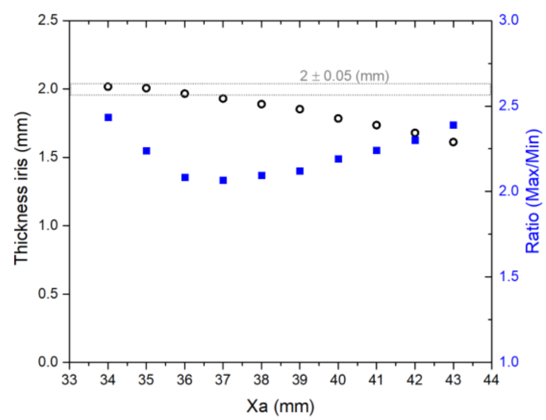

Figure 5. –Iris thickness and max/min ratio are represented against the anode ring distance (Xa) after 175 hours of plating.

The distance from the ring anode to the mask (Xa) was optimised by a parameter sweep simulation. A 2D geometry mesh was used because of the model cylindrical geometry. The SCD module and deformed mesh geometry were coupled for the simulation. The simulation time was fixed to 175 hours and the resulting values of thickness at the equator and iris for each Xa were collected. Afterwards, the thickness at the iris and the ratio between the thickness at the equator and the thickness at the iris were represented as a function of the distance to the equator mask (Xa) (Figure 5). The goal is to achieve the most uniform thickness distribution on the cavity. Thus, the ratio (represented in blue) should be as close as possible to unity. From figure 5, we conclude that the distance Xa of 36 mm gives the minimum of the ratio and provides a sufficient thickness of 2 mm on the iris.

A distance of 36 mm from the anodes to the mask was fixed. The thickness distribution of the optimised assembly after 175 hours of plating is represented in Figure 6.a. In Figure 6.b is presented the thickness distribution on the cavity without optimisation. The results are taken from the 2D model by applying a 3D revolution on the symmetry axis. The results show the effective thickening of the iris when the optimised mask and anodes are used compared with the reference case.

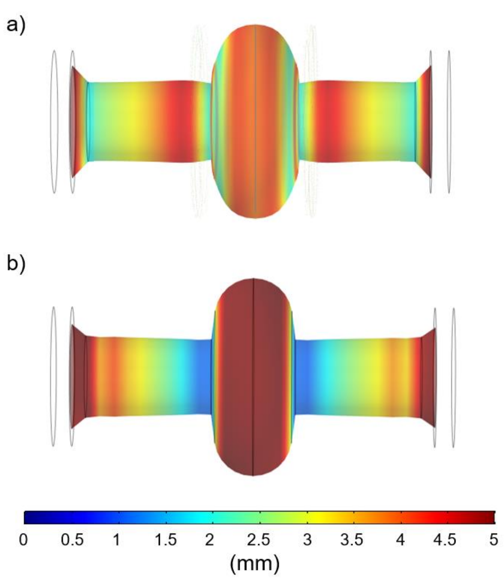

Figure 6. - Electroformed copper thickness distribution (in mm) along the cavity after electroplating for 175 hours at 1.6A/dm2: a) with secondary anodes; b) without secondary anodes.

The anodic dissolution at the secondary anodes was also assessed. In our case, we can study the current lines and geometry of the anodes at the initial (Figure 7.a) and the final stage (Figure 7.b) of the 175 hours of plating. In this arrangement, the current lines from the primary anodes (bath) are blocked and dispersed by the presence of the mask at the equator. The current lines, which start on the secondary anodes, contribute for the deposition at the iris and cut-off, but the rear side of the secondary anodes contributes to the deposition of the equator, as well. The consumption of the anodes on this configuration is of around 72 %. The secondary anodes are electrically connected and mechanically supported thanks to an inserted pin, 2 cm depth, on the outer side of the ring. If this anode is heavily consumed, the connection to the pin will be lost. Therefore, it is a risk if the process consumes more than 2/3 of the annular anodes. In addition, the current that is used on the secondary anodes cannot be independently controlled from the one that is used on the main anodes, when both are connected at the same potential. If the current density at the secondary anodes rises too much, that may lead to the passivation of the copper anodes hindering their function to provide copper where it is most needed. To avoid this, a secondary power supply can be used to independently control the voltage and current at the secondary anodes. In this arrangement, the main power supply is used to connect the sample with the anodes of the bath while the second power supply connects the sample with the secondary anodes (see Figure 8).

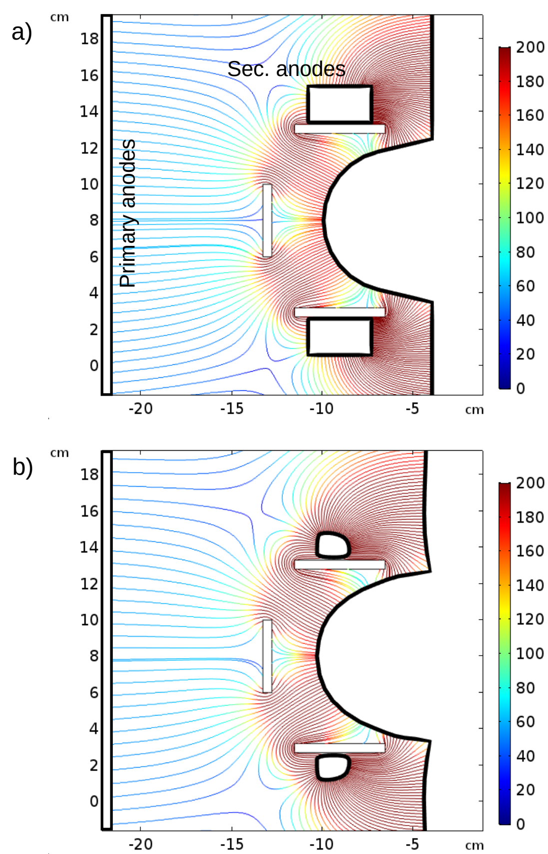

Figure 7. Current line distribution: a) for the initial time (t=0); b) for the final time (175h). The current density of the plating lines is defined by their colours and the equivalent value is shown in the colour bar.

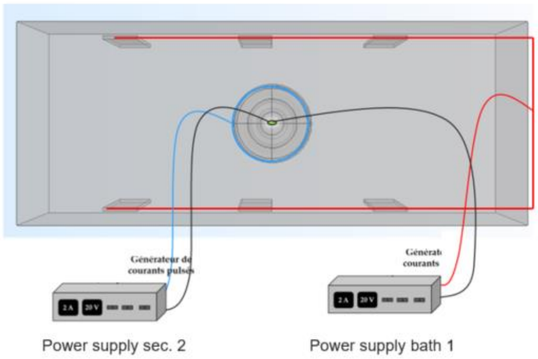

Figure 8. Two power supplies configuration. Power supply 1 is between cathode and the main anodes of the bath. The secondary power supply is between cathode and the secondary anode rings. Each power supply is controlled independently.

In this configuration, the total current is split between the primary and the secondary anodes. Reducing the current density at the secondary anodes will reduce anode consumption. However, the equator to iris thickness ratio and the thickness at the iris have to be re-assessed. A parameter sweep with different current ratio between the primary and secondary anodes was performed to study the electroplating process, keeping the total average current density on the cavity to 1.6 A/dm^2.

Figures 9.a and 9.b show the anodic current density at the secondary anodes and the deformed mesh geometry for the selected ratio of 30% of current on the secondary supply at the initial and end time of the plating (190 hours), respectively. It is compared with the previous case, one power supply after 175 hours of plating. Applying 30% of the total current on the secondary anodes will correspond on the cavity to an average contribution of $0.48 A/dm^2$ and $1.12\ A/dm^2$ from the secondary and primary anodes, respectively. This solution also keeps the anodic dissolution current density below $4 A/dm^2$ during the process and the secondary anode consumption is reduced from 72 % to 32 %.

In the new configuration, the plating time was increased from 175 to 190 hours to ensure a thickness at the iris of 2 mm (as seen in Figure 9.c). A loss in thickness uniformity was expected by reducing the contribution from the secondary anodes, but it is still lower (max/min = 3) than the case without optimisation (max/min = 4.6) that was observed in Figure 1. In addition, the integrity of the secondary anodes is ensured.

Finally, this result also decreases the total plating time from 300 hours (without optimisation) to 190 hours.

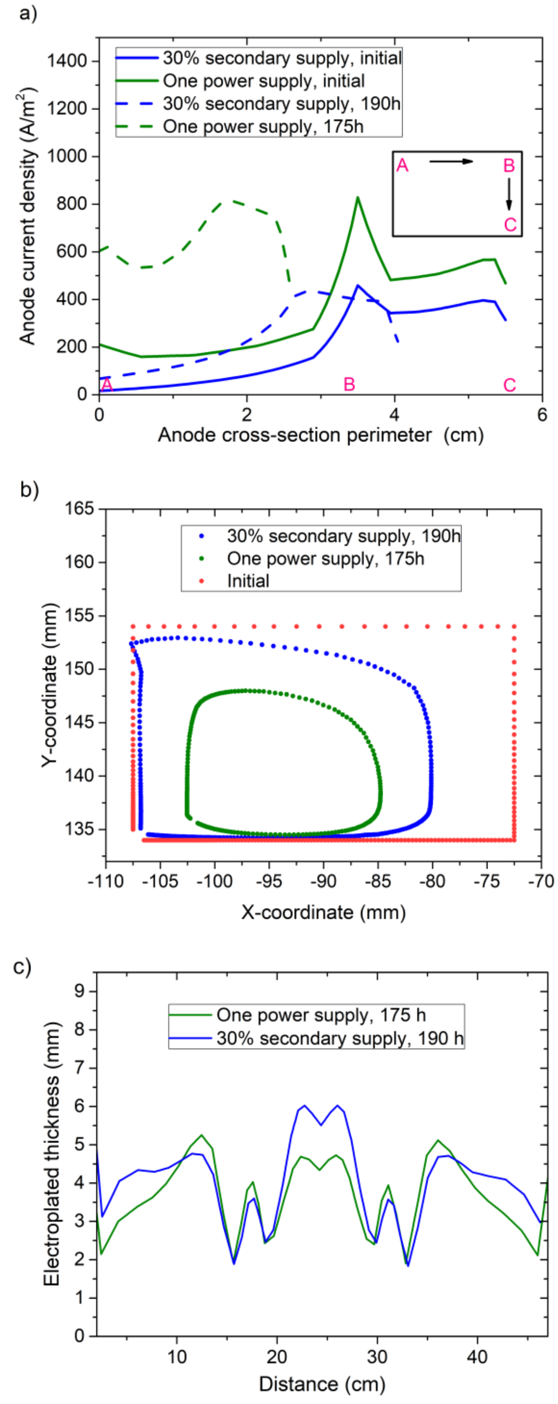

Figure 9. Two power supplies assessment: a) Anode current density for the two different configurations at the start of the plating (full line) and at the end (dotted line); b) Geometry of secondary anodes after plating for the two different configurations; c) Thickness distribution along the cavity for the two different configurations in Figure 8.

4. Conclusions

COMSOL modelling of the electroforming process of the cavity was made to define an optimised geometry of anode and masking that highly improves the copper layer thickness distribution along the cavity and reduces the plating time.

The re-meshing of the anodes helped to identify the anode lifetime and to determine the secondary anode current density. Two power supplies were implemented to control independently the primary and secondary anodes. The current density at the secondary anodes was reduced to minimise anode consumption and the overall control of the process was improved. Future work will focus in validating experimentally the simulated solution.

Acknowledgements

This research is supported by the knowledge transfer (KT) fund at CERN. The research leading to this work is part of the Future Circular Collider study.

References

1. Sublet A. et al. 'Developments on SRF coatings at CERN'. Proceedings of the 17th International conference on RF superconductivity SRF15.

2. V. Palmieri, 'Metal forming technology for the fabrication of seamless superconducting radiofrequency cavities for particle accelerators'. MATEC Web of conferences, 2015.

3. Calatroni S., '20 years of experience with the Nb/Cu technology for superconducting cavities and perspectives for future developments'. Physica C 441, 95-101.

4. Lain Amador L., 'Production of ultra-high vacuum chambers with integrated getter thin film coatings by electroforming'. PhD Thesis. 2019. CERN-THESIS-2019-160.